https://doi.org/10.17221/91/2022-SWR

Detection of high erosion risk areas and their incorporation into environmental impact assessment

Efrén Tarancón-Andrés, Jacinto Santamaria-Peña, David Arancón-Pérez, Eduardo Martínez-Cámara, Julio Blanco-Fernández*

Department of Mechanical Engineering, University of La Rioja, Logroño, La Rioja, Spain

**Corresponding author: eduardo.martinezc@unirioja.es*

Citation: Tarancón-Andrés E., Santamaria-Peña J., Arancón-Pérez D., Martínez-Cámara E., Blanco-Fernández J. (2023): Detection of high erosion risk areas and their incorporation into environmental impact assessment. Soil & Water Res., 18: 102–115.

Abstract: Life Cycle Assessment (LCA) is normally used independently of the physical and temporal location of the product, process or service under analysis. This makes LCA results more easily comparable and globally accepted. At the same time, it has drawbacks though, e.g. land use will have the same impact regardless of location. However, the use of certain terrains in high erosion risk areas as compared to others in low erosion risk areas will have a different impact on the ecosystem. The availability of airborne Light Detection and Ranging (LiDAR) data (ALS) allows a quick and accurate morphogeometric analysis of any terrain. For this reason, this article offers a methodology, based on Revised Universal Soil Loss Equation (RUSLE) method and airborne LiDAR data, for the straightforward detection of zones with high vulnerability to erosion problems. Based on these local erosion risk data, a method is developed to assess the environmental impact of land use, based on its location. In this way, the LCA methodology is incorporated to gather local data, dependent on the specific location of the activity under analysis. The methodology developed has been applied, as a case study, to a specific municipality in the high mountains of the Autonomous Community of La Rioja (Spain).

Keywords: environmental impact; land use; LiDAR; life cycle assessment; soil erosion

The term ecosystem services comprises all the resources and services provided by the ecosystem that benefit human beings (Adhikari & Hartemink 2016). Within these ecosystem services, four different categories have been established. The first category includes provisioning services such as food for human consumption, freshwater, timber or fuel. Another category refers to regulation services, such as erosion, water and gas regulation, climate regulation or the regulation of biological processes such as pollination or diseases. The next category is the cultural services provided by the ecosystem. The fourth category includes the support services that make the production of the three previous categories of ecosystem services viable.

A key element to maintain these ecosystem services is the soil and the erosive processes it may undergo (Pimentel & Kounang 1998). Land erodability can be defined as the resistance of its soil to the processes of disintegration and crumbling of particles (Rueda et al. 2010). Rainfall is often considered to be the main soil erosion agent (Pimentel & Kounang 1998), which is why special attention is paid to the rain-soil relationship and its erosive effects (Lee & Hsu 2021). Furthermore, it is generally accepted that the erodability of soil will depend greatly on its physical and chemical properties, although the type of vegetation cover has a decisive influence as well (Zhou et al. 2008; Çomakli & Turgut 2021; Kabelka et al. 2021). Another significant aspect to consider is land slope. With all other aspects set equal for comparison, it stands logical to assume that runoff processes will be particularly significant when the terrain is too steep (Mohammed et al. 2020; Fan et al. 2022). In addition, terrain orientation can also be a determining factor, as the

https://doi.org/10.17221/91/2022-SWR

areas most exposed to the sun (in northern latitudes, those facing south) will tend to lose their vegetation and moisture more easily (Oorthuis et al. 2020), thus favouring these erosive processes.

Over the years, different methods have been developed to determine soil erosion. This covers from the Erosion Potential Model (EPM) (Gavrilovic 1962) to the European Soil Erosion Model (EUROSEM) (Morgan et al. 1998), including the Water Erosion Prediction Project (WEPP) (Laflen et al. 1991) and the Soil and Water Assessment Tool (SWAT) (Arnold et al. 2012). However, the most used and cited ones within the scientific literature are the Universal Soil Loss Equation (USLE) (Wischmeier et al. 1958) and the Revised Universal Soil Loss Equation (RUSLE) (Renard et al. 1996).

Light Detection and Ranging (LiDAR) data provide complete and continuous information on the orography of a territory and on the existence or absence of vegetation cover and its size (Sultan Mahmud et al. 2021). Dense point clouds allow geometric modelling of the existing vegetation (MDS) and the terrain itself (DTM). Therefore, by strictly analysing this material, it is possible to discover which areas of the territory are most prone to erosion processes. For instance, Đomlija et al. (2019)used LiDAR data to identify different erosive processes in Vinodol Valley in Croatia.

Moreover, it is significant to assess, not only the potential erosion risk, but also the possible impact of erosion on ecosystem services. Life Cycle Assessment (LCA) is one of the most widely used tools to assess the environmental impact of products, services and processes (Guinée et al. 2002; Rebitzer et al. 2004; ISO 14040:2006; ISO 14044:2006). LCA has been applied in fields as diverse as construction (Pleșcan et al. 2022) agriculture (Koellner et al. 2013; Scuderi et al. 2021) and the energy sector (Llantoy et al. 2021). It is commonly used independently of the physical and temporal location of the product, process or service under analysis. This makes LCA results more easily comparable and globally accepted. It has drawbacks though, e.g. land use will have the same impact regardless of location. However, the use of certain terrains in high erosion risk areas, as compared to others in low erosion risk areas, will have a different impact on the ecosystem (Pimentel & Kounang 1998). Pavan and Ometto (2018) emphasize on the significant contribution of ecosystem services to human well-being, as well as the importance of the soil as provider of a great variety of services. Within this context, Pavan and Ometto (2018) indicate the need of generating new indicators to measure and assess the contribution of the aforementioned ecosystem services in LCA. Bearing these assumptions in mind, this article presents a swift method to detect high erosion risk areas over large terrains, using the RUSLE method and LiDAR data. Based on these local erosion risk data, a method is developed to assess the environmental impact of land use based on its location. The methodology developed has been applied, as a case study, to a specific municipality in the high mountains of the Autonomous Community of La Rioja (Spain), taking the data generated during 2016 as base material, with an average resolution of 2 points/m^2.

MATERIAL AND METHODS

Study area

The study area includes 8 km^2 of a mountainous area from North Spain (Figure 1), with altitudes between 899 and 1 958 m a.s.l. (Figure 2A). The typical vegetation cover in the study area includes permanent meadows, hardwood forests and conifers, without significant crop areas.

At a geological level, the area is underlain by Mesozoic sediments, which generate silty-clay soils with a high calcium carbonate content and shallow depth. The climate is temperate, oceanic, Sub-Mediterranean, with annual precipitation values over 900 mm and a maximum 24-hour precipitation (with a return period of 10 years) over 70 and 100 mm/24 h.

The study area (Figure 2B) includes a South zone with high sandstones and slates and a North zone with siliceous conglomerates. The central study zone shows a higher variability containing schists and slates, conglomerates, red clays, marls and gypsums, chalcedonies, dolomitic limestone breccias and dolostones, limestone banks and dolostones, clays, sands and angular edges and gravels, sands and shales.

Erosion risk determination

To determine the terrain's erosion susceptibility, the RUSLE method was used. This method is based on the combination of five factors, according to Equation 1.

$$A = R \times K_{fs} \times LS \times C \times P \quad (1)$$

where:

A – mean annual soil loss (t·h^{-1}·year^{-1});

R – erodibility factor due to rainfall intensity (MJ·mm·ha·h^{-1}·year^{-1});

https://doi.org/10.17221/91/2022-SWR

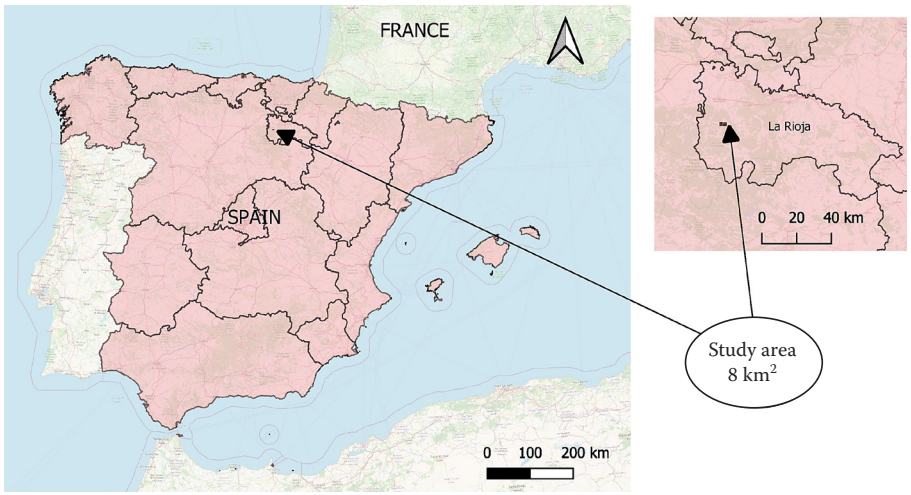

Figure 1. Geographical location of the study area

K – soil erodibility factor (t·ha·h·ha^{-1}·MJ^{-1}·mm^{-1});
LS – dimensionless topographic factor derived from the length and the steepness of the slopes;
C – dimensionless factor of terrain vegetation cover;
P – dimensionless factor of the soil conservation practices.

R factor. The rain erodibility R factor defines the water input, which will generate the erosive processes with a higher influence on soil loss (Renard 1992).

This R factor has been obtained from the data series from 1960 to 1996 provided by the Ministry of Agriculture, Fishing and Food (MAPA in Spanish) with

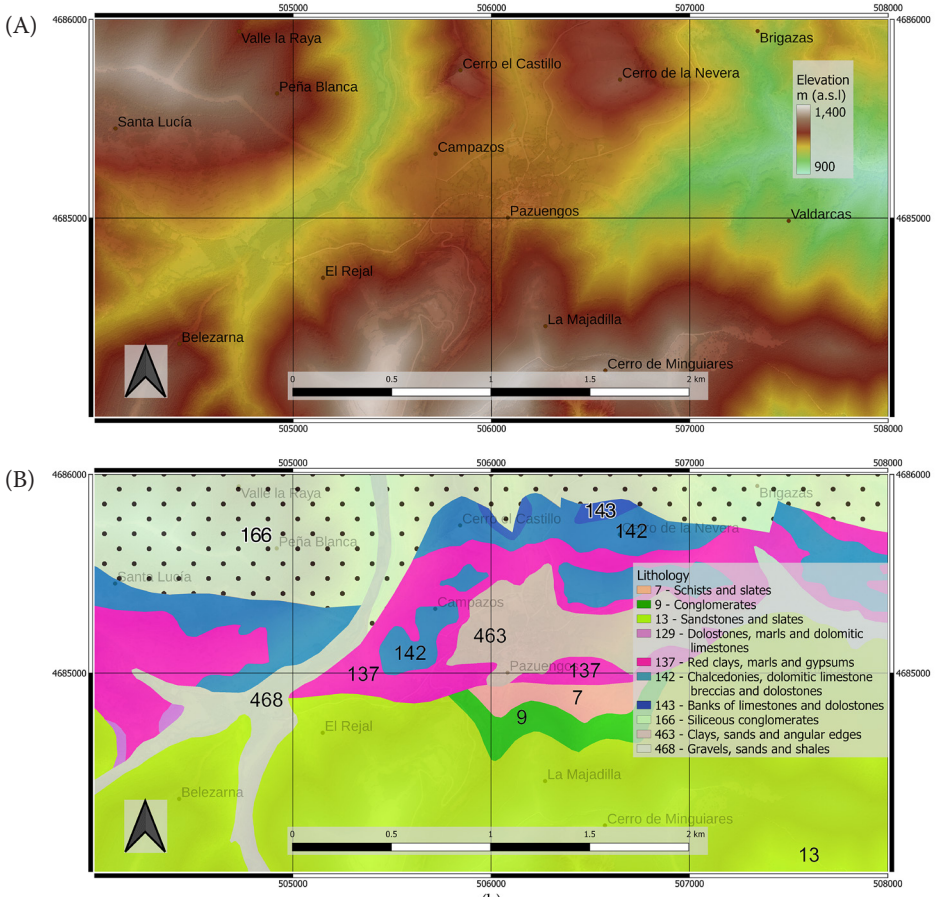

Figure 2. Elevation map (A) and geological map (B) of the study area
Source: Instituto Geologico y Minero de España (Geology and Mining Institute of Spain 1980)

https://doi.org/10.17221/91/2022-SWR

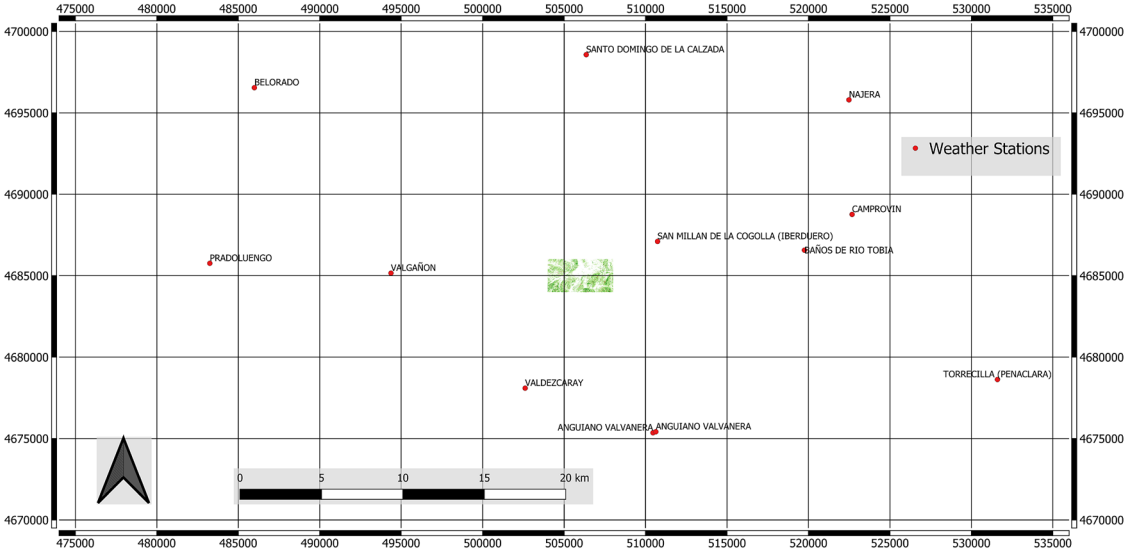

Figure 3. Weather stations located within a 15 km radius of the area under study and used to R factor calculation
R – erodibility factor due to rainfall intensity

geostatistical interpolation methods (kriging), in turn provided by the data from 3 591 stations belonging to the network from the State Weather Agency (AEMET in Spanish) (Ministry of Agriculture Fishing and Food 2022). Eight of these 3 591weather stations are located within a 15 km radius of the area under study (Figure 3). The R factor calculation was based on the study of "Aggressiveness of Rain in Spain" (Ministry of Agriculture Fishing and Food 1988) published by the Ministry of Agriculture, Fishing and Food. With the creation of a data bank, processing pluviographs and rainfall information, this study obtained the R factor with regression equations, using rainfall and zoning variables of the monthly distribution of the R factor. The R factor was calculated following Equation (2) developed by Wischmeier and Smith (1978):

$$R = \sum_{12}^{1} 1.735 \times 10^{\left(1.5 \log_{10}\left(\frac{P_i}{P}\right) - 0.08188\right)} \quad (2)$$

where:
P_i – monthly rainfall (mm);
P – annual rainfall (mm).

The R factor of the study area is shown in Figure 4.

K_{fs} factor. Data from the International Soil Reference Information Centre (ISRIC 2022) have been

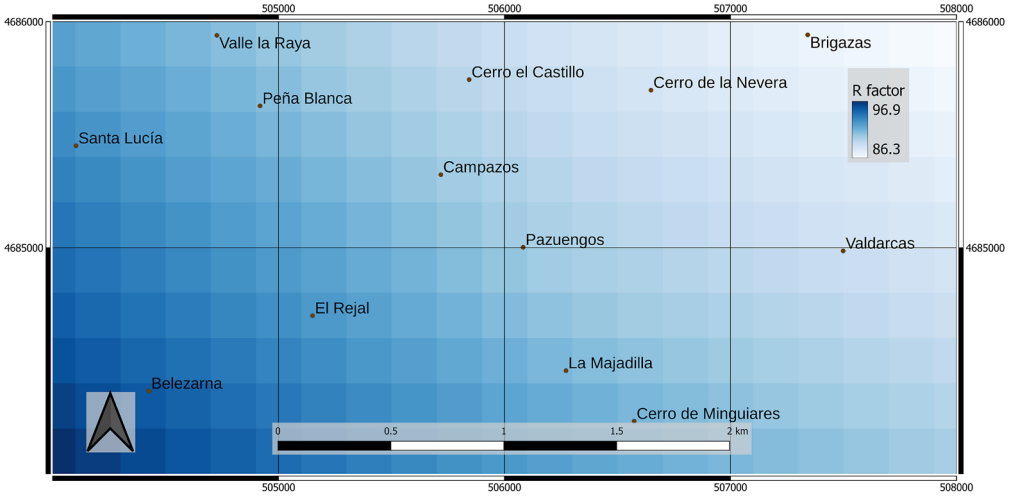

Figure 4. R factor map of the study area
R – erodibility factor due to rainfall intensity

https://doi.org/10.17221/91/2022-SWR

used to calculate the K factor, using the following soil properties from 0 to 30 cm: clay, sand; silt and soil organic matter.

The input data used to calculate the K factor has been obtained from the SoilGrids system. SoilGrids is based on open source principles and allows researchers to access detailed soil data information. The database developed in the SoilGrids Project incorporates world-wide data from 6 million georeferenced records, to obtain a comprehensive catalogue of soil profile data. The data available in SoilGrids (Hengl et al. 2017) can be obtained with a resolution of 250 m and includes datasets of different soil properties at seven depths (0, 5, 15, 30, 60, 100 and 200 cm).

Notwithstanding, only clay, sand, silt and soil organic matter properties up to a depth of 30 cm have been used.

Based on these data, the equations defined by Neitsch et al. (2000) have been used to calculate the K factor:

$$\mathrm{K} = 0.1317 \times f_{\mathrm{Sand}} \times f_{\mathrm{Clay}} \times f_{\mathrm{SOC}} \times f_{\mathrm{Silt}} \tag{3}$$

$$f_{\mathrm{Sand}} = \left(0.2 + 0.3 \times e^{-0.256 \times m_{\mathrm{Sand}} \times \left(1 - \frac{m_{\mathrm{Silt}}}{100}\right)}\right) \tag{4}$$

$$f_{\mathrm{Clay}} = \left(\frac{m_{\mathrm{Silt}}}{m_{\mathrm{Clay}} + m_{\mathrm{Silt}}}\right)^{0.3} \tag{5}$$

$$f_{\mathrm{SOC}} = \left(1 - \frac{0.0256 \times \mathrm{OrgC}}{\mathrm{OrgC} + e^{(3.72 - 2.95 \times \mathrm{OrgC})}}\right) \tag{6}$$

$$f_{\mathrm{Silt}} = \left(1 - \frac{0.7 \times \left(1 - \frac{m_{\mathrm{Sand}}}{100}\right)}{\left(1 - \frac{m_{\mathrm{Sand}}}{100}\right) + e^{\left(-5.51 + 22.9 \times \left(1 - \frac{m_{\mathrm{Sand}}}{100}\right)\right)}}\right) \tag{7}$$

where:

m_{Sand} – proportion (%) of sand content;

m_{Silt} – proportion (%) of silt content;

m_{Clay} – proportion (%) of clay content;

OrgC – proportion (%) of organic carbon content.

The K factor of Equation (3) does not consider the content effect of rock fragments in the soil and, therefore, may give results that are far from reality in certain areas, especially if they are mountainous (Brooks et al. 2014). To avoid this problem, the possible effect of rock fragment contents on soil erodibility has also been included, according to the equations of Yang et al. (2023):

$$St = 1 - 1\, e^{-0.04\,(Rc - 10)} \tag{8}$$

$$\mathrm{K}_{fs} = (1 - St) \times \mathrm{K}) \tag{9}$$

where:

St – mean relative rill sediment yield;

Rc – cover of rock fragments on the soil surface (%);

K_{fs} –factor of the study area (Figure 5).

LS factor. To determine the topographic factor, slope length, steepness factor (LS) and LiDAR

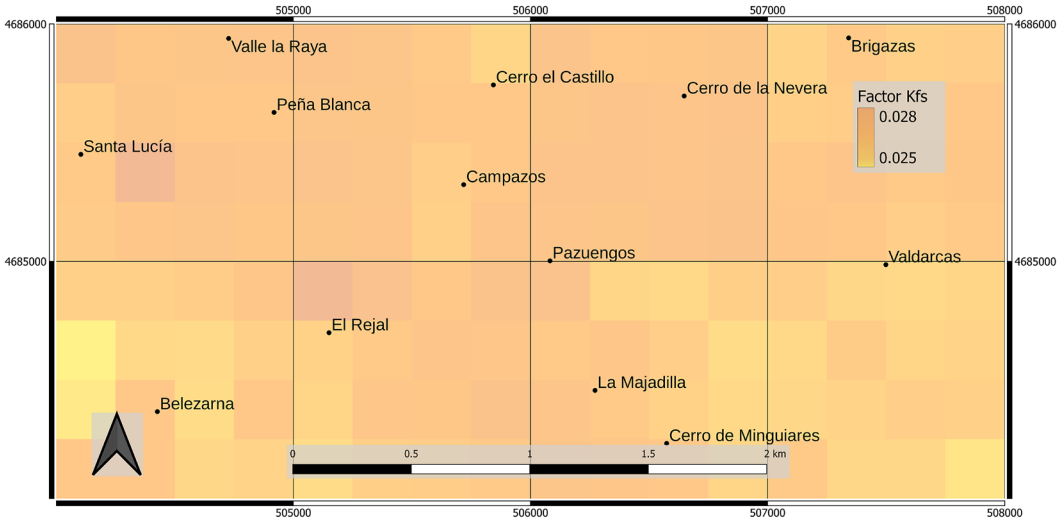

Figure 5. Map of the soil erodibility factor of the study area (K_{fs})

https://doi.org/10.17221/91/2022-SWR

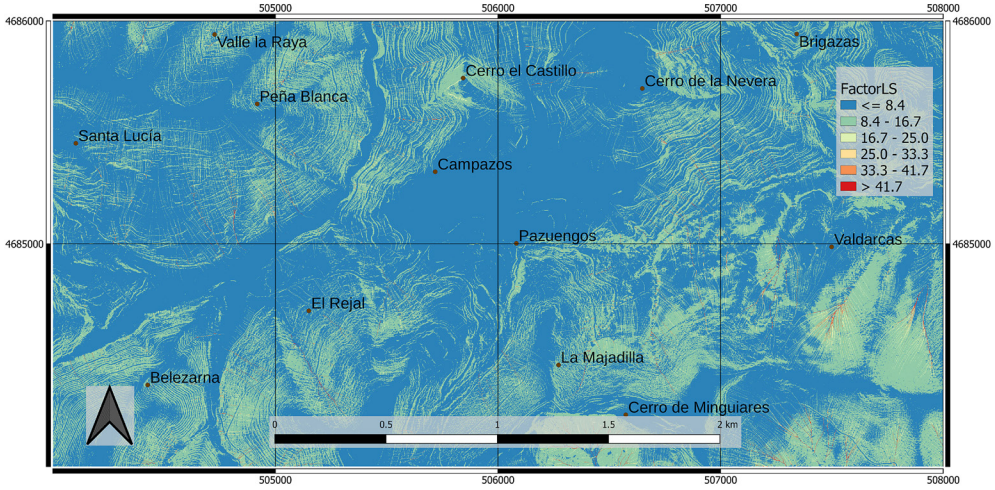

Figure 6. LS factor map of the study area
LS – topographic factor derived from the length and the steepness of the slopes

data were used. In this case, sheets 504-4 686 and 506-4 686 of the LiDAR flight performed in 2016 by the Government of La Rioja are used, covering a total area of 8 km^2 (2 × 4 km). The LiDAR point cloud datasets used in this work were downloaded from the Spatial Data Infrastructure of the Government of La Rioja accessible from IDERioja Portal. These datasets are freely available, fully covering the regional territory of La Rioja (IDERioja 2016). The average density of the point cloud obtained were about 2 points/m^2, with altimetry precisions of RMSE < 20 cm, the total number of points being 16 620 171. The points are already classified in the categories established by the American Society for Photogrammetry and Remote Sensing (ASPRS) for files in LAZ format (Lohani & Mishra 2009).

Slope factor (McCool et al. 1989; Desmet & Govers 1996) has been calculated according to the following equations:

$$L = \frac{\left(A_{i,j} + D^2\right)^{m+1} - A_{i,j}^{m+1}}{D^{m+2} \times x_{i,j}^{m} \times 22.13^{m}} \quad (10)$$

$$m = \left(\frac{F}{1+F}\right) \quad (11)$$

$$F = \left(\frac{\frac{\sin\beta}{0.0896}}{3\times(\sin\beta)^{0.8} + 0.56}\right) \quad (12)$$

$$S = \begin{cases} 10.8\times \sin\beta + 0.03 \;, \beta < 0.09 \\ 16.8\times \sin\beta - 0.5 \;, \beta \geq 0.09 \end{cases} \quad (13)$$

where:
β – slope angle in degrees;
$A_{i,j}$ – area considered in the input mesh;
D – size of the mesh;
$x_{i,j}$ – sum of the orientation sine and cosine;
m – slope-length exponent;
F – ratio between rill erosion and interrill erosion.

The LS factor of the study area is shown in Figure 6.

C factor. The C factor determines the effect of vegetation in the soil erosion processes. The LiDAR data of the study area also allow estimating a C factor value based on the normalized difference vegetation index (NDVI). The LiDAR flight of the Autonomous Community of La Rioja was made in September 2016, with a point density of 2 pulses/m² together with oblique RGB and near infrared photographic images. The NDVI can be calculated based on the following equation:

$$NDVI = \frac{NIR - RED}{NIR + RED} \quad (14)$$

where:
NIR – near infrared band;
RED – red band of the multispectral images.

Following the methodology of García-Gutiérrez et al. (2010) the use of the intensity data (I) from the LIDAR data has been proposed as an approximation to the NIR to obtain the NDVI, according to the following equation:

$$NDVI = \frac{I - RED}{I + RED} \quad (15)$$

The two necessary bands have been extracted using the GIS program and the NDVI index has been

https://doi.org/10.17221/91/2022-SWR

calculated for the area under study, based on the LIDAR data used to calculate the LS factor. The NDVI index values vary from –1 to 1, with higher index values indicating the presence of vegetation in the area.

With this index, the C factor (Van der Knijff et al. 2000) can be obtained based on Equation (16):

$$C = e^{-\alpha \times \left(\frac{NVDI}{\beta - NDVI}\right)} \quad (16)$$

where:

α, β – dimensionless parameters that define the relation between the NDVI and the C factor (α = 2 and β = 1).

This C factor estimation is based on the total integrated vegetation canopy cover via remote sensing and, therefore, cannot differentiate between ground cover and tree cover.

The C factor of the study area is shown Figure 7.

P factor. The P factor determines how the soil conservation practices affect the water currents and their impact in soil erosion. Kouli et al. (2009) highlight the importance of different agricultural practices in erosion control. They define a value of 0, for the cases in which an appropriate anthropic erosion control is used and a value of 1 when anthropic erosion control is not conducted. The P factor value ranges between 1 and 0. For the study area, a uniform value of 1 has been used for the whole study.

The idea presented in the article was to use a methodology relatively quick and easy to perform, with widely available global data. It is certainly possible to improve the erosion risk estimation in the area by incorporating land use. However, that would also involve the use of data that may not be as readily available and would hinder an otherwise relatively easy and accessible application of the methodology. This is the main reason why a value of 1 has been used for the P factor throughout the study.

Erosion risk map. The combination of the different factors analysed in the previous sections facilitates determining the areas most prone to erosion processes due to the cumulative effect of unfavourable conditioning factors.

Therefore, the annual erosion index allows establishing erosion risk criteria in the different regions under study. In this case, a fixed criterion is used (Ministry of Agriculture Fishing and Food 2008) based on the significant amount of potential erosion by hectare and year, calculated through the RUSLE method using 2016 LIDAR data:

Low risk: ≤ 2 t·ha^{-1}·year^{-1}

Moderate risk: ≤ 12 t·ha^{-1}·year^{-1}

High risk: ≤ 25 t·ha^{-1}·year^{-1}

Very high risk: >25 t·ha^{-1}·year^{-1}

The Spanish National Action Program against Desertification establishes three desertification risk categories: periods of less than 12, 12–25 t·ha^{-1}·year^{-1} and more than 25 t·ha^{-1}·year^{-1}. Based on the parameters of the aforementioned categories, four erosion risk criteria have been established for this article.

In this way, an erosion risk scale, from 1 to 4, is obtained based on the combined characteristics of each of the points analysed in the area under study.

Determination of the characterisation factor according to erosion risk

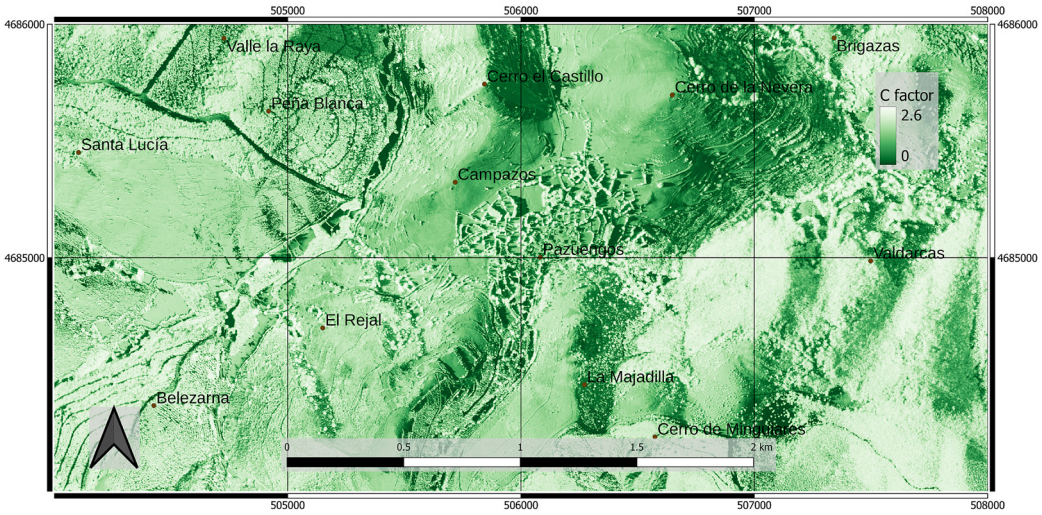

Figure 7. C factor map of the study area

C – dimensionless factor of the soil conservation practices

https://doi.org/10.17221/91/2022-SWR

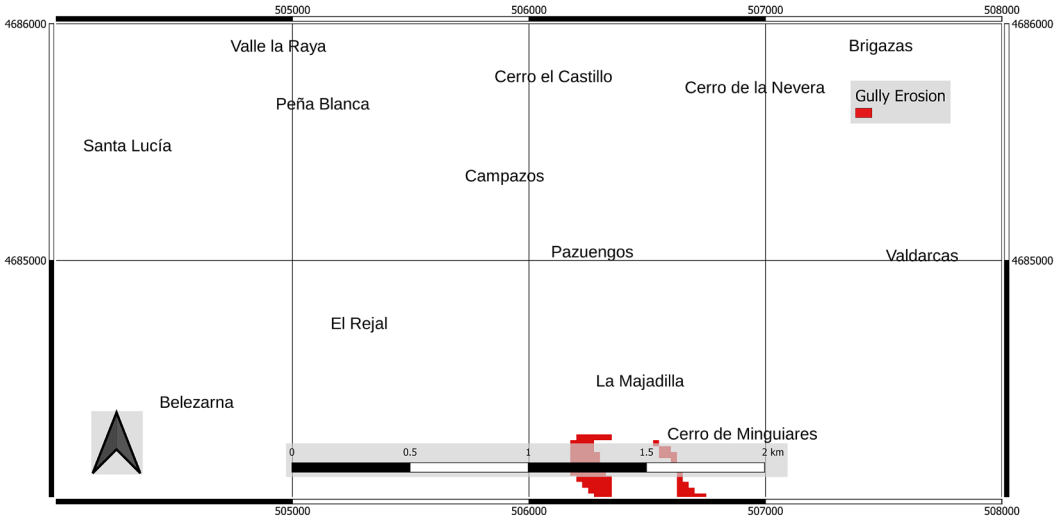

Figure 8. Gully erosion locations of the study area

To determine the characterization factor to be applied, according to the soil erosion risk, the criteria followed were those of the 2008 National Action Programme against Desertification (Ministry of Agriculture Fishing and Food 2008). Based on the four erosion risk levels defined above, four characterisation factors ranging from 1 to 4 were established.

In addition, it was necessary to identify those locations where ravine erosion has occurred as high erosion risk areas (Shellberg 2021). In the case of the area under study, the location of these ravine erosions can be seen in Figure 8. These areas have been obtained from the National Soil Erosion Inventory of Spain.

These characterization factors are linked to the erosion risk of each region, obtained from the GIS data. In this sense, the calculation of the environmental impact will be affected by the specific land use location, and will therefore consider the specific local characteristics with respect to the erosion risk of that land.

Determination of the environmental impact of land use according to the erosion risk

The integration of erosion risk in the LCA requires creating an environmental impact assessment method that can be incorporated into the Life Cycle Impact Assessment (LCIA) phase. In this LCIA phase, the different environmental impacts of each impact category under study are evaluated, for example: abiotic depletion, global warming potential for a 100-year time horizon, ozone layer depletion, human toxicity, fresh water aquatic ecotoxicity, marine aquatic ecotoxicity, terrestrial ecotoxicity, land use, photochemical oxidation, acidification, or eutrophication. In order to perform this assessment for each impact category, the characterization factors that apply to each entry of the Life Cycle Inventory (LCI), collected for the LCA, must be established. For the environmental impact assessment method proposed in this article, these characterization factors have been established in point 2.3 and are applied based on the erosion risk, in the area in which the land is to be occupied.

Land use is one of the environmental impact categories usually analysed in the LCA. The land use impact category used for the LCA methodology evaluates the environmental impact of the occupation, alteration and management of the land for human activities (Brentrup et al. 2002).

The environmental impact assessment method for land use, according to the erosion risk, has been defined according to Equation (17):

$$\mathrm{LCIA}_{\mathrm{Erosion}} = \frac{\mathrm{Area}_{\mathrm{LCI}_{\mathrm{Land\ Use}}}}{\mathrm{Area}_{\mathrm{Region}\ i}} \times t \times \mathrm{CF}_i \qquad (17)$$

where:

$\mathrm{Area}_{\mathrm{LCI\ LandUse}}$ – size of the occupied land in m^2;

$\mathrm{Area}_{\mathrm{Regioni}}$ – size in m^2 of the land occupation region;

t – occupation time in years;

CF_i – characterisation factor of the land occupation region.

The units of the proposed LCIA are: m^2 LCI activity × m^{-2} Region i × y. Núñez et al. (2010) propose a method for assessing the environmental impact of desertification, similar to the one proposed in this article, for the case of erosion.

https://doi.org/10.17221/91/2022-SWR

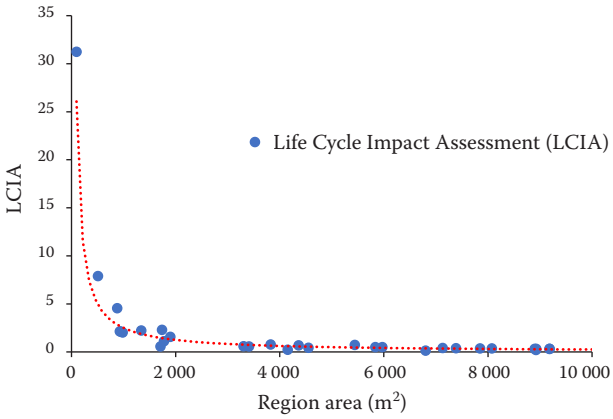

Figure 9. Environmental impact according to the area of the region in which the one-year, 1 000 m^2 land occupation takes place

This calculation methodology allows weighing the impact according to the size of the region, in a way that, for the same land occupation, there will be more impact if the region in question is smaller. For instance, Figure 9 shows the impact evolution calculated for a 1 000 m^2 land occupation for one year, in different erosion risk regions.

RESULTS AND DISCUSSION

Erosion risk map. Based on the factors defined by the RUSLE method, an erosion risk map has been generated.

The final results obtained are shown in Figure 10.

The superimposition of the analysis conducted on the study area allows the identification and planimetry of the action areas (Figure 11), which are necessary to define the characterisation factors that allow the environmental impact to be calculated, according to the specific land location.

Figure 10 shows red areas that denote a very high erosion risk, dark green areas that represent a high erosion risk and light green areas that mark a medium erosion risk. Areas in white indicate that low risk factors are present.

Table 1 shows the regions found according to erosion risk. Eight regions have been found in the very high erosion risk category (erosion risk 4), with areas ranging from 2 741 080 to 506 m^2. In the high erosion risk category (erosion risk 3), there are 27 regions with areas ranging from 425 045 to 96 m^2. In the medium erosion risk category (erosion risk 2), there are 17 regions ranging from 871 113 to 927 m^2. Three regions have been found with low erosion risk factors (erosion risk 1), ranging from 6 799 to 1 706 m^2.

The results show that out of a total of 800 ha initially studied, 536.7 ha have been identified as very high erosion risk areas, due to the adverse conditions in these areas. In this study, these areas represent around 67.0% of the territory studied and are grouped into eight different regions.

A total of 146.9 ha were found to be at high risk of erosion, representing 18.3% of the land analysed.

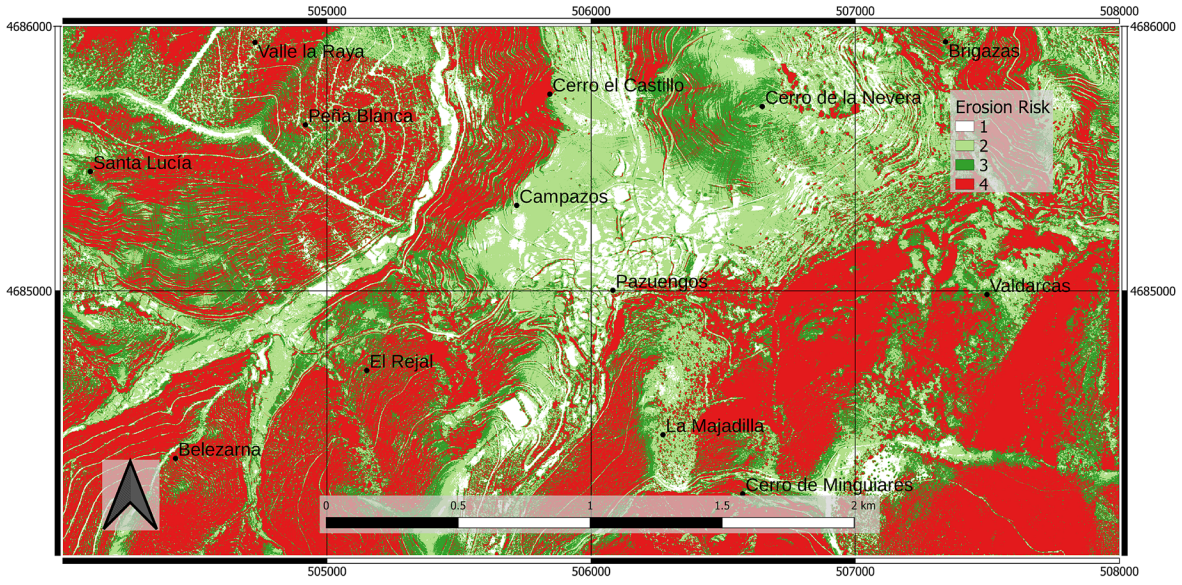

Figure 10. Classification of zones by risk factors
The red areas are the ones showing the highest rates in the risk factors considered

https://doi.org/10.17221/91/2022-SWR

These high erosion risk areas are distributed in 27 regions with a significant variation in size.

The medium erosion risk areas represent 14.5% of the studied land and account for a total of 116.3 ha distributed in 17 regions.

Environmental impact of land use. Based on the erosion risk map and the four types of regions defined in it, an assessment can be made of the environmental impact of a given land use in different areas of the region under study.

For example, if eight possible locations are studied for the installation of a farm, the environmental impact could be analysed in the category of land use, proposed in this article. From this point of view, the best location could be determined.

For this case study, a 1 000 m^2 land occupation is assumed in different locations in the four types of regions defined according to the erosion risk (Table 2). The scenarios proposed in this case study, include the occupation of two different regions in each of the four erosion risk zones (very high, high, medium and low risk). For each risk zone, two different-sized regions have been selected to assess the effect of the region size according to the occupation made.

As shown in the different cases presented as examples, an important factor in determining the impact is the land occupation size, as compared to the total size of the region. This reflects the notion that the larger the land occupied relative to the total size of the region, the greater its environmental impact should be.

Table 1. Area of the different regions according to their erosion risk

Erosion risk 1		Erosion risk 2		Erosion risk 3		Erosion risk 4	
Region	area	region	area	region	area	region	area
1	1 706	1	3 304	1	96	1	5 439
2	4 151	2	12 762	2	4 361	2	33 234
3	6 799	3	927	3	8 926	3	46 200
		4	29 285	4	23 157	4	506
		5	4 552	5	217 275	5	878
		6	980	6	7 130	6	2 741 080
		7	13 458	7	75 170	7	2 538 196
		8	1 776	8	9 180	8	1 736
		9	871 113	9	7 848		
		10	12 488	10	98 897		
		11	116 141	11	74 952		
		12	34 854	12	1 340		
		13	3 407	13	20 981		
		14	942	14	9 182		
		15	8 921	15	1 896		
		16	26 447	16	5 971		
		17	21 812	17	73 643		
				18	8 072		
				19	3 823		
				20	182 879		
				21	11 496		
				22	5 834		
				23	86 200		
				24	8 897		
				25	89 673		
				26	425 045		
				27	7 386		
Total	12 656		1 163 169		1 469 310		5 367 269

https://doi.org/10.17221/91/2022-SWR

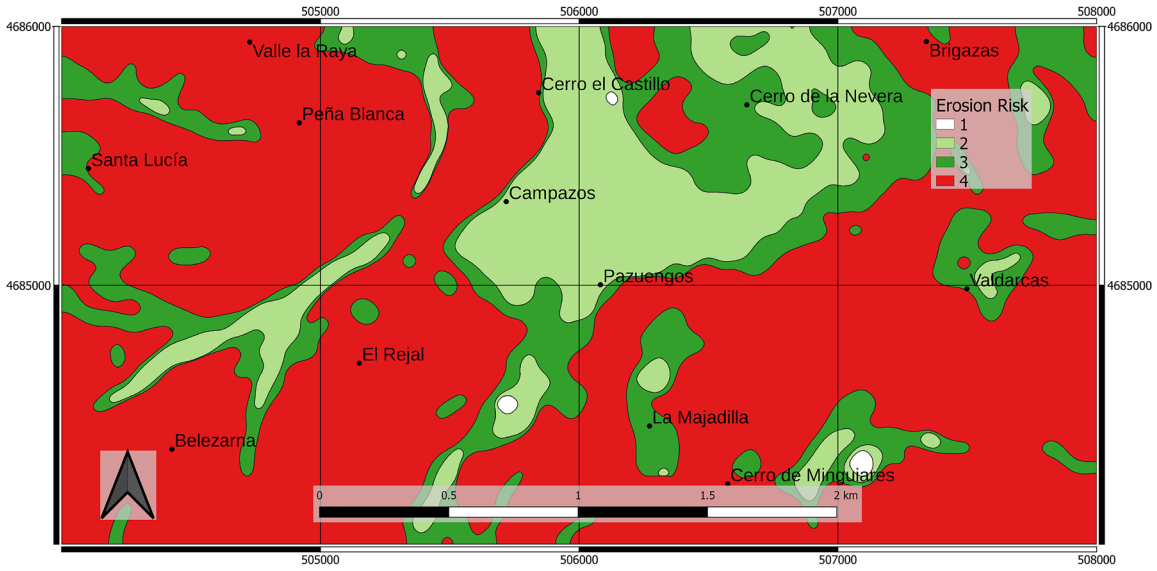

Figure 11. Identification of regions according to erosion risk

On the other hand, there is also a clear effect of the type of region in which the land is occupied. The results show that the characterization factor ensures that land occupation in higher erosion risk areas will have a greater environmental impact in the category of land use proposed in this article. This can be asserted as long as the relationship between the size of the occupied land and the region in which it is located is maintained.

In these examples, it can be seen how easily an environmental impact assessment of land use can be applied, considering the specific aspects of the terrain location. In this particular case, an assessment is made of the erosion risk of the specific region where the land use will occur. The power of GIS systems and the increasingly abundant cartographic information available facilitates developing environmental impact assessment methodologies that consider local aspects of the specific location where the work occurs.

The proposed methodology has some weak points, such as the fact that it does not consider the cumulative effect of other existing land occupations. Furthermore, in the case of the P factor, including soil conservation practices, a global value of 1 has been established for the whole area under study, to simplify the application of the methodology. In this way, a simpler and faster methodology is achieved, without the need of accessing more complex data from the area under study, which can be hard to find. In turn, valuable information is lost, which could be otherwise used to calculate the erosion risk in more detail, based on the soil conservation applied to each area.

Table 2. Environmental impact of a 1 000 m^2 plot of land in different regions according to erosion risk

Region erosion risk	Region area (m^2)	Land use (m^2)	Characterization factor	Time (year)	LCIA ($m^2 \times m^2 \times$ year)
4	1 736	1 000	4	1	2.30E+00
4	33 234	1 000	4	1	1.20E-01
3	1 896	1 000	3	1	1.58E+00
3	20 981	1 000	3	1	1.30E-01
2	1 776	1 000	2	1	1.13E+00
2	21 812	1 000	2	1	9.17E-02
1	1 706	1 000	1	1	5.86E-01
1	6 799	1 000	1	1	1.47E-01

LCIA – life cycle impact assessment

https://doi.org/10.17221/91/2022-SWR

One of the main disadvantages of the LCA methodology is that it lacks temporal resolution (Finnveden et al. 2009; Zamagni et al. 2009). This implies that the life cycle inventories used to represent average and aggregate data in a permanent temporal regime. Therefore, they do not include dynamic considerations or temporal evolutions that may affect the real environmental impact.

On the other hand, the proposed methodology does not differentiate between ground cover and tree cover. Ground cover, such as grass and shrubs, has particular relevance in erosion control. Therefore, it would be advisable to include this differentiation according to the type of cover for future developments of the methodology proposed in this article.

CONCLUSION

By means of airborne LiDAR data (ALS) and using specific processing software, erosion risk factors maps can be obtained to, once integrated into a Geographic Information System, detect the areas of greater or lesser risk of erosive processes. This will make it possible to conduct environmental impact assessments that consider those areas that, given their geomorphology and current vegetation cover, are at greater risk of erosion and are affected to a greater extent by the land-use activities being analysed.

The methodology developed defines a method for assessing the environmental impact of land use according to the erosion risk of the specific terrain where the activity is performed. The methodology is easy to apply and based on current widely available data.

For governments and official institutions, the described methodology can be a useful tool for the detection of areas with high vulnerabilities in terms of soil erosion risks and for the environmental impact assessment of future activities to be implemented in such areas.In general, these institutions have the necessary materials at their disposal, as there are relatively recent flights over the whole territory and with sufficient densities, which enables them to swiftly and accurately locate risk areas over large portions of the territory and incorporate them into the environmental impact assessment methodology proposed in this article.

REFERENCES

Adhikari K., Hartemink A. E. (2016): Linking soils to ecosystem services – A global review. Geoderma, 262: 101–111.

Arnold J.G., Moriasi D.N., Gassman P.W., Abbaspour K.C., White M.J., Srinivasan R., Santhi C., Harmel R.D., Van Griensven A., Van Liew M.W. (2012): SWAT: Model use, calibration, and validation. Transactions of the ASABE, 55: 1491–1508.

Brentrup F., Küsters J., Lammel J., Kuhlmann H. (2002): Life Cycle Impact assessment of land use based on the hemeroby concept. The International Journal of Life Cycle Assessment, 7: 339–348.

Brooks A., Spencer J., Borombovits D., Pietsch T., Olley J. (2014): Measured hillslope erosion rates in the wet-dry tropics of Cape York, northern Australia: Part 2, RUSLE-based modeling significantly over-predicts hillslope sediment production. Catena, 122: 1–17.

Çomakli E., Turgut B. (2021): Determining the effects of the forest stand age on the soil quality index in afforested areas: A case study in the Palandöken mountains. Soil and Water Research, 16: 237–249.

Desmet P.J.J., Govers G. (1996): A GIS procedure for automatically calculating the USLE LS factor on topographically complex landscape units. Journal of Soil and Water Conservation, 51: 427–433.

Đomlija P., Gazibara S.B., Arbanas Ž., Arbanas S.M. (2019): Identification and mapping of soil erosion processes using the visual interpretation of Lidar imagery. ISPRS International Journal of Geo-Information, 8: 438.

Fan X., Fan H., Dong S. (2022): The coupling of hillslope- and gully-erosion increases their controlling efforts: A case study in Liaoning Province, China. Soil and Water Research, 17: 123–137.

Finnveden G., Hauschild M.Z., Ekvall T., Guinée J., Heijungs R., Hellweg S., Koehler A., Pennington D., Suh S. (2009): Recent developments in Life Cycle Assessment. Journal of Environmental Management, 91: 1–21.

García-Gutiérrez J., Martínez-Álvarez F., Riquelme J.C. (2010): Using remote data mining on LIDAR and imagery fusion data to develop land cover maps. Lecture Notes in Computer Science (Including Subseries Lecture Notes in Artificial Intelligence and Lecture Notes in Bioinformatics), 6096 LNAI(PART 1), 378–387. https://doi.org/10.1007/978-3-642-13022-9_38/COVER

Gavrilovic S. (1962): A method for estimating the average annual quantity of sediments according to the potency of erosion. Bulletin of the Faculty of Forestry, 26: 151–168.

Geology and Mining Institute of Spain (1980): Geological Map of Spain – Sheet 21. Madrid, IGME: 1–27.

Guinée M., Heijungs R., Huppes G., Kleijn R., Koning A. de, Oers L. van, Wegener Sleeswijk A., Suh S., Udo de Haes H.A., Bruijn H. de, Duin R. van, Huijbregts M.A.J., Gorrée J.B. (2002): Handbook on Life Cycle Assessment:

https://doi.org/10.17221/91/2022-SWR

Operational Guide to the ISO Standards. I: LCA in Perspective. IIa: Guide. IIb: Operational Annex. III: Scientific Background. Dordrecht, Kluwer Academic Publishers.

Hengl T., Mendes de Jesus J., Heuvelink G.B. M., Ruiperez Gonzalez M., Kilibarda M., Blagotić A., Shangguan W., Wright M.N., Geng X., Bauer-Marschallinger B. (2017): SoilGrids250m: Global gridded soil information based on machine learning. PLoS ONE, 12: e0169748.

IDERioja (2016): LiDAR flight of the Autonomous Community of La Rioja 2016. Available at https://www.iderioja.larioja.org/cartografia/index.php?map=RIOJA_C04&&&lang=es (assecced Apr 15, 2022).

ISRIC (2022): SoilGrids250 m: Global Gridded Soil Information. Available at https://data.isric.org/geonetwork/srv/eng/catalog.search#/home (accessed March 5, 2022).

Kabelka D., Kincl D., Vopravil J., Vráblík P. (2021): Impact of cover crops in inter-rows of hop gardens on reducing soil loss due to water erosion. Plant, Soil and Environment, 67: 230–235.

Koellner T., Baan L., Beck T., Brandão M., Civit B., Margni M., Canals L. M., Saad R., Souza D. M., Müller-Wenk R. (2013): UNEP-SETAC guideline on global land use impact assessment on biodiversity and ecosystem services in LCA. International Journal of Life Cycle Assessment, 18: 1188–1202.

Kouli M., Soupios P., Vallianatos F. (2009): Soil erosion prediction using the Revised Universal Soil Loss Equation (RUSLE) in a GIS framework, Chania, Northwestern Crete, Greece. Environmental Geology, 57: 483–497.

Laflen J.M., Lane L.J., Foster G.R. (1991): WEPP: A new generation of erosion prediction technology. Journal of Soil and Water Conservation, 46: 34–38.

Lee M.H., Hsu I.P. (2021): Estimation of annual mean rainfall erosivity based on hourly rainfall data in a tropical region. Soil and Water Research, 16: 74–84.

Llantoy N., Zsembinszki G., Palomba V., Frazzica A., Dallapiccola M., Trentin F., Cabeza L. F. (2021): Life cycle assessment of an innovative hybrid energy storage system for residential buildings in continental climates. Applied Sciences (Switzerland), 11: 3820.

Lohani B., Mishra R.K. (2009): Las and lasutility. GIM International, 23: 13–15.

McCool D.K., Foster G.R., Mutchler C.K., Meyer L.D. (1989): Revised slope length factor for the Universal Soil Loss Equation. Transactions of the ASAE, 32: 1571–1576.

Ministry of Agriculture Fishing and Food (1988): Aggressiveness of Rain in Spain. Madrid, ICONA: 1–39. (in Spanish)

Ministry of Agriculture Fishing and Food (2008): National Action Programme against Desertification. Madrid, CCD: 1–36. (in Spanish)

Ministry of Agriculture Fishing and Food (2022): Spatial Data Infrastructure, and Catalog of Inspire Water Visualization Services. Available at https://www.miteco.gob.es/es/cartografia-y-sig/ide/directorio_datos_servicios/agua/wms-inspire-agua.aspx (accessed Apr 20, 2022). (in Spanish)

Mohammed S., Abdo H.G., Szabo S., Pham Q.B., Holb I.J., Linh N.T.T., Anh D.T., Alsafadi K., Mokhtar A., Kbibo I. (2020): Estimating human impacts on soil erosion considering different hillslope inclinations and land uses in the coastal region of Syria. Water, 12: 2786.

Morgan R.P.C., Quinton J.N., Smith R.E., Govers G., Poesen J.W.A., Auerswald K., Chisci G., Torri D., Styczen M.E. (1998): The European Soil Erosion Model (EUROSEM): A dynamic approach for predicting sediment transport from fields and small catchments. Earth Surface Processes and Landforms: The Journal of the British Geomorphological Group, 23: 527–544.

Neitsch S.L., Arnold J.G., Kiniry J.R., Williams J.R. (2000): Erosion Soil and Water Assessment Tool. Theoretical Documentation. Version 2009. Temple, Texas Agricultural Experiment Station. Available at https://swat.tamu.edu/media/99192/swat2009-theory.pdf

Núñez M., Civit B., Muñoz P., Arena A.P., Rieradevall J., Antón A. (2010): Assessing potential desertification environmental impact in life cycle assessment. Part 1: Methodological aspects. The International Journal of Life Cycle Assessment, 15: 67–78.

Oorthuis R., Vaunat J., Hürlimann M., Lloret A., Moya J., Puig-Polo C., Fraccica A. (2020): Slope orientation and vegetation effects on soil thermo-hydraulic behavior. An experimental study. Sustainability, 13: 14.

Pavan A.L.R., Ometto A.R. (2018): Ecosystem Services in Life Cycle Assessment: A novel conceptual framework for soil. Science of the Total Environment, 643: 1337–1347.

Pimentel D., Kounang N. (1998): Ecology of soil erosion in ecosystems. Ecosystems, 1: 416–426.

Pleșcan C., Barta M., Maxineasa S.G., Pleșcan E.L. (2022): Life cycle assessment of concrete pavement rehabilitation: A Romanian case study. Applied Sciences (Switzerland), 12: 1769.

Rebitzer G., Ekvall T., Frischknecht R., Hunkeler D., Norris G., Rydberg T., Schmidt W.P., Suh S., Weidema B.P., Pennington D.W. (2004): Life cycle assessment Part 1: Framework, goal and scope definition, inventory analysis, and applications. Environment International, 30: 701–720.

Renard K.G. (1992): Computerized calculations for conservation planning. Agricultural Engineering, 73: 16–17.

Renard K.G., Foster G.R., Weesies G.A., McCool D.K., Yoder D.C. (1996): Predicting Soil Erosion by Water: A Guide

https://doi.org/10.17221/91/2022-SWR

to Conservation Planning with the Revised Universal Soil Loss Equation (RUSLE). Agriculture Handbook No. 703, Washington D.C., USDA.

Rueda E.B., Cerdà A., González B.S., Viqueira F.D.-F., Delgado J.L.R., Varela M.E., Alleres M.R. (2010): Methods for Studying Soil Erodibility: Their Application in Soils Affected by Forest Fires. Update on Methods and Techniques for Studying Soils Affected by Forest Fires. Valencia, Cátedra Divulgación de la Ciencia, Universidad de Valencia: 85–107.

Scuderi A., Cammarata M., Branca F., Timpanaro G. (2021): Agricultural production trends towards carbon neutrality in response to the EU 2030 Green deal: Economic and environmental analysis in horticulture. Agricultural Economics (Czech Republic), 67: 435–444.

Shellberg J.G. (2021): Agricultural development risks increasing gully erosion and cumulative sediment yields from headwater streams in Great Barrier Reef catchments. Land Degradation & Development, 32: 1555–1569.

Sultan Mahmud M., Zahid A., He L., Choi D., Krawczyk G., Zhu H. (2021): LiDAR-sensed tree canopy correction in uneven terrain conditions using a sensor fusion approach for precision sprayers. Computers and Electronics in Agriculture, 191: 106565.

Van der Knijff J.M., Jones R.J.A., Montanarella L. (2000): Soil Erosion Risk: Assessment in Europe. European Soil Bureau, European Commission Brussels.

Wischmeier W.H., Smith D.D. (1978): Predicting Rainfall Erosion Losses: A Guide to Conservation Planning. Agricultural Handbook No. 537, Science and Education Administration, USDA.

Wischmeier W.H., Smith D.D., Uhland R.E. (1958): Evaluation of factors in the soil loss equation. Agricultural Engineering, 39: 458–462.

Yang M., Yang Q., Zhang K., Wang C., Pang G., Li Y. (2023): Effects of soil rock fragment content on the USLE-K factor estimating and its influencing factors. International Soil and Water Conservation Research, 11: 263–275.

Zamagni A., Buttol P., Buonamici R., Masoni P., Guinée J.B., Huppes G., Heijungs R., van der Voet E., Ekvall T., Rydberg T. (2009): D20 Blue Paper on Life Cycle Sustainability Analysis. Deliverable 20 of Work Package 7 of the CALCAS Project. Project No. 037075 2009, Leiden University.

Zhou P., Luukkanen O., Tokola T., Nieminen J. (2008): Effect of vegetation cover on soil erosion in a mountainous watershed. Catena, 75: 319–325.

Received: June 21, 2022
Accepted: April 17, 2023
Published online: May 2, 2023